A genome-wide MAGIC kit for recombinase-independent mosaic analysis in *Drosophila*

Yifan Shen[1], Ann T. Yeung[1,2], Payton Ditchfield[3], Elizabeth Korn, Rhiannon Clements, Xinchen Chen[4], Bei Wang, Michael Sheen[5], Parker A. Jarman[6], and Chun Han*

Department of Molecular Biology and Genetics, Cornell University, Ithaca, New York, USA

Weill Institute for Cell and Molecular Biology, Cornell University, Ithaca, New York, USA

[1]These authors contributed equally.

[2]Current address: Harvard Medical School, Boston, MA 02115, USA

[3]Current address: Center for Community Independence, Revere, MA 02151, USA

[4]Current address: Department of Neurobiology, School of Biological Sciences, University of California, San Diego, La Jolla, CA 92093, USA.

[5]Current address: Warren Alpert Medical School of Brown University, Providence, RI 02903, USA

[6]Current address: Yale School of Medicine, New Haven, CT 06510, USA

*For correspondence: chun.han@cornell.edu (CH)

ABSTRACT

Mosaic analysis has been instrumental in advancing developmental and cell biology. Most current mosaic techniques rely on exogenous site-specific recombination sequences that need to be introduced into the genome, limiting their application. Mosaic analysis by gRNA-induced crossing-over (MAGIC) was recently developed in *Drosophila* to eliminate this requirement by inducing somatic recombination through CRISPR/Cas9-generated DNA double-strand breaks. However, MAGIC has not been widely adopted because gRNA-markers, a required component for this technique, are not yet available for most chromosomes. Here, we present a complete, genome-wide gRNA-marker kit that incorporates optimized designs for enhanced clone induction and more effective clone labeling in both positive MAGIC (pMAGIC) and negative MAGIC (nMAGIC). With this kit, we demonstrate clonal analysis in a broad range of *Drosophila* tissues, including cell types that have been difficult to analyze using recombinase-based systems. Notably, MAGIC enables clonal analysis of pericentromeric genes and deficiency chromosomes and in interspecific hybrid animals, opening new avenues for gene function study, rapid gene discovery, and understanding cellular basis of speciation. This MAGIC kit complements existing systems and makes mosaic analysis accessible to address a wider range of biological questions.

33 **INTRODUCTION**

34 Mosaic animals containing genetically distinct populations of cells in the same organism are
35 useful for *in vivo* studies of complex biological processes. For this reason, techniques that can
36 generate genetically labeled mosaic clones have been utilized in both vertebrates and
37 invertebrates to study tissue-specific functions of pleiotropic genes, developmental timing, cell
38 lineages, cell proliferation, neural wiring, and many other biological phenomena [1-3]. The most
39 popular mosaic techniques rely on site-specific recombination systems, such as FRT/Flp [4, 5]
40 and LoxP/Cre [6, 7], to induce somatic recombination between homologous chromosomes. Such
41 techniques require the introduction of recombination sites to specific locations in the genome and
42 thus cannot be applied to unmodified chromosomes. To overcome this limitation, we recently
43 developed a recombinase-independent mosaic technique called mosaic analysis by gRNA-
44 induced crossing-over (MAGIC) [8]. In MAGIC, the CRISPR/Cas9 system generates double-
45 strand breaks (DSBs) at a predefined genome location to induce homologous recombination in
46 precursor cells during S/G2 phase. Subsequent chromosomal segregation during mitosis can
47 result in clones homozygous for the chromosomal segments distal to the crossover site. Two
48 variants of this technique in *Drosophila*, positive MAGIC (pMAGIC) and negative MAGIC
49 (nMAGIC), label the resulting homozygous clones by the presence and absence of fluorescent
50 markers, respectively [8]. Like FRT/Flp-based techniques, MAGIC enables characterization of
51 homozygous clones of lethal mutations in otherwise heterozygous animals [8].

52 However, unlike FRT/Flp-based techniques, MAGIC does not require prior genetic
53 modification of the test chromosome. Thus, it can potentially be used on any chromosome and
54 have much wider applications. Foremost, mutations of diverse natures have been established for
55 most *Drosophila* genes [9-14], and thousands of deficiency strains harbor deletions that
56 collectively uncover 98.4% of the *Drosophila* genome [15]. However, most of these mutant
57 chromosomes cannot be analyzed by traditional mosaic techniques due to the lack of FRT sites
58 or incompatibility with the FRT/Flp system. In contrast, MAGIC can theoretically be applied to
59 these chromosomes as they are, allowing convenient genome-wide mosaic screens. In addition,
60 genes located more proximal to centromeres than existing FRT sites cannot be analyzed by
61 FRT/Flp techniques. In comparison, MAGIC can potentially be used to study these genes
62 because the crossover site in MAGIC can be flexibly defined by users. Lastly, given that
63 MAGIC is compatible with wild-derived chromosomes [8], it may be able to generate

64 homozygous clones of a chromosome derived from a single species in an interspecific hybrid
65 animal, allowing the study of species-related cell-cell interactions.

66 Despite these potentials, MAGIC has not been widely adopted by the *Drosophila*
67 community. A major barrier is the lack of gRNA-marker transgenes on most chromosomal arms,
68 which are necessary for DSB induction and fluorescent clone labeling [8]. In addition, the
69 existing gRNA-markers suffer from several limitations, including low frequency of clone
70 induction, weak labeling of pMAGIC clones, and suboptimal visualization of nMAGIC clones.
71 Because of these reasons, MAGIC has only been successfully applied to a few genes in a limited
72 number of *Drosophila* tissues [8, 16].

73 To overcome these limitations, here we first optimized gRNA-marker designs to improve
74 clonal induction, the brightness of pMAGIC clones, and visualization of nMAGIC clones. Then
75 we generated pMAGIC and nMAGIC gRNA-markers for all chromosomal arms and
76 characterized their ability to generate clones. Using this kit, we demonstrate mosaic analysis of
77 centromere-proximal genes, deficiency chromosomes, chromosomes derived from different
78 *Drosophila* species in interspecific hybrid animals. This kit allows optimal clone induction in
79 diverse cell and tissue types and should be useful for studying a wide range of biological
80 processes.

81 **RESULTS**

82 **New gRNA-marker designs improve pMAGIC and nMAGIC**

83 MAGIC relies on a gRNA-marker dual-transgene (Figure 1A) inserted in a specific
84 chromosomal arm to both induce and visualize clones homozygous for this arm [8]. The gRNA
85 part of the construct expresses two gRNAs ubiquitously to target a pericentromeric location on
86 this arm. Two gRNAs targeting two sequences that are close to each other, instead of a single
87 gRNA, are used to increase the probability of DSBs and thus the clone frequency. The marker
88 part in pMAGIC utilizes a ubiquitously expressed Gal80 to prevent Gal4-dependent labeling of
89 heterozygous and homozygous cells for the gRNA-marker, while allowing labeling of
90 homozygous cells that lose the gRNA-marker. In contrast, nMAGIC uses ubiquitously expressed
91 BFP, which results in brighter labeling of gRNA-marker homozygous cells, intermediate
92 labeling of gRNA-marker heterozygous cells, and lack of labeling of gRNA-marker-negative
93 homozygous cells.

94 We have previously developed gRNA-marker vectors for both pMAGIC and nMAGIC.
95 However, gRNA-markers made with these vectors exhibit some limitations. First, the clone
96 frequency can be low for certain gRNAs [8]. Second, the *ubi-Gal80* in pMAGIC gRNA-markers
97 does not completely suppress Gal4 activity in certain tissues, such as hemocytes. Third,
98 pMAGIC clones are sometimes too dim to visualize cell morphology, such as thin dendrite and
99 axon projections of neurons. Lastly, nMAGIC utilizes a nuclear BFP marker (nlsBFP), which
100 does not show the cell shape and sometimes cannot mark clones effectively. Thus, to optimize
101 MAGIC, we first sought to improve the gRNA-marker designs.

102 Since clone induction in MAGIC depends on gRNA-induced DNA DSBs, we asked
103 whether a more efficient gRNA design enhances clone frequency in somatic tissues. The
104 previous gRNA-marker vectors used a tgFE design, which contains the "F+E" gRNA scaffold
105 and a $tRNA^{Gly}$ before each gRNA targeting sequence (Figure 1A) [8]. However, we have shown
106 that an improved Qtg2.1 design, which contains the gRNA2.1 scaffold and a single $tRNA^{Gln}$
107 spacer between the two gRNAs (Figure 1A), is much more mutagenic than tgFE in somatic
108 tissues [17]. We thus compared two pMAGIC gRNA-markers that are based on these two gRNA
109 designs but target the same genomic sequences at cytological band 40D2 to assess their ability to
110 induce clones in peripheral sensory neurons. When used with the same neuronal/epidermal
111 precursor Cas9, *zk-Cas9* [8], Qtg2.1 resulted in three times more neuronal clones as compared to
112 tgFE (Figure 1B), confirming a positive correlation between gRNA efficiency and clone
113 frequency.

114 To ensure more complete suppression of Gal4 activity by Gal80 in pMAGIC, we
115 replaced the *ubi* enhancer driving Gal80 expression with an *αTub84B* (*tub*) enhancer that was
116 used in *tub-Gal80* in the MARCM system [18]. When combined with the larval hemocyte
117 marker *pxn-Gal4 UAS-CD4-tdTom* [19] (Figure 1C), *ubi-Gal80* did not completely suppress the
118 labeling of hemocytes (Figure 1D). In contrast, no labeled hemocytes could be detected in the
119 presence of *tub-Gal80* (Figure 1E), suggesting that *tub-Gal80* is a better marker for pMAGIC.

120 To improve clone brightness in pMAGIC, we sought to destabilize Gal80 and reduce its
121 expression, reasoning that dim clones are due to prolonged Gal80 activity after clone induction.
122 In addition to replacing the *ubi* enhancer with the *tub* enhancer, we also introduced protein and
123 mRNA destabilization sequences (DE) [20, 21] at the 3' end of the Gal80 coding sequence, and

124 replaced the *His2Av* polyA by *SV40* polyA (Figure 1F), as the latter reduces transgene
125 expression [22]. By measuring the brightness of epidermal (Figure 1G) and neuronal (Figure 1H)
126 clones induced by *gRNA-40D2* and *gRNA-42A4*, we found that each of the three changes
127 improved clone brightness.

128 Lastly, to visualize cell shape in nMAGIC, we replaced nlsBFP with cytosolic BFP
129 tagged by 3X Hemagglutinin (HA), in addition to utilizing the *tub* enhancer. This new design
130 allowed us to better discern clone shapes in both the wing imaginal disc and the epidermis
131 (Figure 1J, 1J', and 1L), in contrast to the previous *ubi-nlsBFP* design (Figure 1I and 1K).

132 Thus, by altering the designs of the gRNAs and the Gal80 and BFP markers, we created
133 new vectors optimized for more robust applications of nMAGIC and pMAGIC.

134 **A gRNA-marker kit is established for all four chromosomes of *Drosophila***

135 To enhance the utility of MAGIC in *Drosophila*, we generated complete sets of pMAGIC and
136 nMAGIC gRNA-markers for all four chromosomes (Figure 2A). To identify suitable gRNA
137 target sites, we analyzed the pericentromeric sequences of X, 2L, 2R, 3L, 3R, and 4, based on
138 three criteria [8]: conserved in closely related *Drosophila* species to minimize the chance of
139 single nucleotide polymorphism, (2) located away from functionally critical regions to avoid
140 disrupting essential processes, and (3) unique within the genome to minimize off-target effects.
141 For each MAGIC construct, we selected a pair of non-repetitive gRNA target sequences in
142 intergenic regions to maximize the chances of DSBs. These two sequences are closely linked to
143 minimize the risk of large deletions. Given the variable efficiency of gRNA target sequences, we
144 selected three pairs of gRNAs targeting three chromosomal locations for each chromosomal arm
145 and named them according to the corresponding cytoband (Table 1).

146 To evaluate the clone-induction properties of these gRNAs, we combined the pMAGIC
147 set with *zk-Cas9* and counted the number of neuronal clones in A1-A7 larval hemi-segments
148 (Figure 2B). As expected, the clone frequency varied from gRNA to gRNA, but we were able to
149 identify efficient gRNAs for every chromosomal arm. We previously found that different gRNAs
150 follow the same trend of relative efficiency in different tissues [8]. Here we additionally tested
151 nMAGIC gRNAs for 2R in the wing disc (Figure 2C) and noticed a similar trend of clone
152 induction to that of their pMAGIC counterparts in sensory neurons (Figure 2B), suggesting that
153 the results in sensory neurons are transferrable to other tissues.

154 Certain gRNAs (e.g. gRNA-40E1) exhibited very low clone frequency. Such gRNAs can
155 be useful for inducing sparse clones in highly packed issues such as the brain. For example,
156 using the same *ey-Cas9* [23], the highly efficient gRNA-40D2 induced too many neuronal clones
157 in the adult brain for morphological analysis (Figure 2D), while gRNA-40E1 gave rise to few
158 clones, whose projection patterns were much easier to analyze (Figure 2E).

159 Together, the pMAGIC and nMAGIC gRNA-marker lines constitute a complete kit
160 (Table 1) for genome-wide MAGIC applications in *Drosophila*.

161 **MAGIC allows clonal analysis in diverse tissues and cell types**

162 To determine if MAGIC can be applied to diverse tissues in *Drosophila*, we conducted clonal
163 analysis in the larva using *gRNA-40D2(Gal80)* and several tissue-specific Cas9s. With the
164 ubiquitous *vas-cas9* [24] and *tub-Gal4 UAS-mCD8-GFP*, we readily detected clones in the larval
165 brain (Figure 3A), proliferating tissues like eye and leg discs (Figure 3B-C), and polyploid
166 tissues like the fat body, gut, and trachea (Figure 3D-F). Clone induction in polyploid tissues
167 suggests that crossing-over events occurred before the last cell division. Using *zk-cas9* and
168 *R38F11-Gal4>UAS-tdTomato (tdTom)*, we observed frequent epidermal clones (Figure 3G).
169 Using the glia precursor *gcm-Cas9* and *repo-Gal4>UAS-mCD8-GFP*, we detected individual
170 glial clones in the brain (Figure 3H). Lastly, the new pMAGIC gRNA-marker design allowed us
171 to reliably induce hemocyte clones (Figure 3I). These results collectively demonstrate MAGIC's
172 efficacy in generating clones in diverse *Drosophila* tissues, indicating its value in studying gene
173 function and cell lineage in various tissue contexts.

174 The neuromuscular junction (NMJ) in *Drosophila* larvae has been a valuable model for
175 elucidating synaptic biology, owing to its simplicity, accessibility, and conserved features shared
176 with mammalian excitatory synapses [25-27]. Despite its popularity, the NMJ has rarely been
177 analyzed by the MARCM technique in the literature, likely due to the difficulty of inducing
178 clones in motor neurons. To test the effectiveness of MAGIC in analyzing gene function at the
179 NMJ, we selected two genes crucial for synaptic function and construction: *Vesicular glutamate*
180 *transporter* (*VGlut*) [28] and *bruchpilot* (*brp*) [29, 30], null mutations of each of which exhibit
181 recessive lethality in larvae. Combined with appropriate gRNA(Gal80) lines (42A4 for *vGluT* on
182 2R and 40D2 for *brp* on 2L) and *tub-Gal4 UAS-CD8-GFP*, *zk-Cas9* induced frequent clones in
183 type Ib boutons (Figure 4A-B"). The loss of vGluT or Brp specifically in GFP-labeled NMJs was

184 confirmed by immunostaining. These results exemplify the value of pMAGIC for dissecting
185 gene function in NMJ biology at the single cell level.

186 **MAGIC enables clonal analysis of pericentromeric genes, 4th chromosome-associated**
187 **mutations, and in interspecific hybrid animals**

188 Because all FRT sites in the existing FRT/Flp mosaic system are located at some distances away
189 from centromeres, it has not been possible to study genes located between the FRT sites and the
190 corresponding centromeres by clonal analysis. In contrast, the gRNA target site in a MAGIC
191 experiment can be user-selected to enable clonal analysis of any given gene. To illustrate this
192 potential, we used *gRNA-41F9* to induce homozygous mutant clones of *Ecdysone receptor*
193 (*EcR*), which is located at 42A10 and is inaccessible to all FRT sites on 2R. EcR is a
194 transcription factor required for neuronal remodeling during metamorphosis [31]. In peripheral
195 sensory neurons, EcR activation at the beginning of pupariation causes apoptosis of some
196 dendritic arborization (da) neurons while triggering dendrite pruning of other da neurons [32]. As
197 expected, a wildtype (WT) pMAGIC clone of class IV da (C4da) neuron exhibited complete
198 dendrite pruning at 16 h after puparium formation (APF), accompanied by dendrite debris
199 phagocytosed into epidermal cells [19] (Figure 5A). In contrast, *EcR* mutant da neuron clones
200 still maintained larval dendritic arbors at 16 h APF (Figures 5B-D), instead of dying (in the case
201 of C3da) or undergoing dendrite pruning (in the cases of C1da and C4da).

202 Mosaic analysis of genes located on the 4th chromosome had not been possible until
203 recent introduction of FRT sites onto this chromosome by CRISPR-mediated knock-in [33].
204 Despite these advances, existing mutations on FRT-lacking 4th chromosomes still cannot be
205 analyzed by the FRT/Flp system. A valuable gene-disruption resource in *Drosophila* is the
206 deficiency library consisting of strains harboring chromosomal deletions. MAGIC can
207 potentially be used in conjunction with the deficiency library to screen for genes important in a
208 particular biological process. To test the potential of MAGIC for analyzing mutations on the 4th
209 chromosome and for gene discovery with deficiencies, we generated pMAGIC C4da clones of
210 *Df(4)ED6380*, a deficiency that deletes a segment between cytological bands 102B7 and 102D5.
211 These clones show dramatically reduced dendrites compared to the WT controls (Figure 4E-4G),
212 indicating the existence of genes important for dendrite growth in this region.

When examining nMAGIC gRNA-markers for the 4th chromosome, we noticed uneven expression of *tub-3xHA-BFP* in epidermal cells and some imaginal tissues, exemplified by cells lacking detectable BFP signal (Figures S1A,S1B). This variegated expression is likely due to transgenes residing in heterochromatin and is common for transgenes located on the 4th chromosome [34]. While this uneven expression limits the usefulness of our gRNA-markers in the corresponding epithelial tissues, Gal80 in pMAGIC gRNA-markers efficiently suppressed Gal4 activities in most neurons (Figure S1C), conforming their effectiveness in neuronal MAGIC analysis.

Lastly, we wondered if the MAGIC system can generate clones in interspecific hybrid animals derived from *D. melanogaster* and *D. simulans* parents, given that the two species show a large degree of synteny [35]. The clones in these animals would contain homozygous chromosomal arms derived from a single species. To test this idea, we crossed *D. melanogaster* females containing *gRNA-42A4(BFP); hh-cas9* to *D. simulans* males carrying a loss of function mutation of *Lethal hybrid rescue mutation* (*Lhr*), which ensures the viability of the hybrid male progeny [36]. Indeed, we observed twin spots consisting of dark clones, containing only *D. simulans* 2R, and brighter clones, containing only *D. melanogaster* 2R, in wing discs of both female and male progeny (Figure 5G and 5H), demonstrating the feasibility of studying species-specific alleles in cell-cell interactions in interspecific hybrids.

DISCUSSION

Conceptually, MAGIC is a simpler and more convenient mosaic technique compared to traditional recombinase-dependent methods. However, the lack of gRNA-marker transgenes has prevented its wide application in *Drosophila*. In this study, we present a complete gRNA-marker kit that enables genome-wide MAGIC in *Drosophila*, removing this bottleneck. The new gRNA-markers incorporate optimized designs that improve clone frequency and labeling in both pMAGIC and nMAGIC. We further demonstrate the compatibility of MAGIC with broad tissues and cell types. More importantly, MAGIC enables mosaic analyses that could not be accomplished by existing FRT/Flp systems, such as those of pericentromeric genes, deficiency chromosomes, and interspecific homologous chromosomes. Thus, this MAGIC kit provides *Drosophila* researchers with greater flexibility for conducting mosaic analyses of diverse purposes.

243 To implement MAGIC, one needs to first choose a proper Cas9 that is expressed in the
244 precursor cells of the targeted cell population. We show that ubiquitously expressed Cas9 lines,
245 such as *vas-Cas9* [24] and *Act5C-Cas9* [37], are sufficient to induce clones in broad tissues.
246 Alternatively, heat shock (HS)-induced Cas9 [38] can offer temporal control of clone induction
247 in most tissues, akin to the HS-Flp commonly used in FRT-based mosaic analysis. The third
248 option is a Cas9 driven by a tissue-specific enhancer specifically in the precursor cells of the
249 target tissues. Examples shown in this study include *ey-Cas9* expressed in many neuronal
250 lineages [23], *gcm-Cas9* expressed in glial progenitor cells [39], *ZK-Cas9* expressed in precursor
251 cells of epidermal cells, motor neurons, and somatosensory neurons [17], and *hh-Cas9* expressed
252 in imaginal tissues [40]. These Cas9 lines have the advantages of being more specific and
253 efficient, and more convenient to use than ubiquitous or inducible ones. Multiple strategies,
254 including enhancer fusion [37, 40], Gal4-to-Cas9 conversion [17, 41], and insertion of Cas9 in
255 specific gene loci [39], have been developed to ease the generation of such tissue-specific Cas9
256 lines. As an ongoing effort, we have been converting Gal4 lines known to be expressed in
257 progenitor cells into Cas9 (available at
258 https://bdsc.indiana.edu/stocks/genome_editing/crispr_cas9.html), in the hope of making
259 MAGIC accessible to more *Drosophila* tissues.

260 The second component of MAGIC is a gRNA-marker line that resides on the appropriate
261 chromosome arm and targets Cas9 to cut a pericentromeric site on the same arm. In the gRNA-
262 marker kit, we generated three lines targeting different sites for each chromosome arm. These
263 lines exhibit a broad range of clone frequencies in larval sensory neurons. As different gRNA-
264 markers maintain similar relative efficiencies of clone induction across tissues [8], one can
265 choose a gRNA-marker more appropriate for their applications based on the target gene location
266 and the desired clone frequency. Notably, a higher clone frequency may not always be
267 beneficial, such as when studying the projection patterns of individual neurons in the brain. A
268 low efficiency gRNA-marker in this kit may be more desirable in such applications.

269 Besides commonly conducted mosaic analysis in *Drosophila*, MAGIC also enables many
270 novel analyses that are difficult or impossible to accomplish with traditional systems. One
271 example is to analyze interactions among species-specific cells in an interspecific hybrid animal
272 for understanding the cell biological basis of hybrid incompatibility. Interspecific crosses
273 between WT *D. melanogaster* and WT *D. simulans* result in sex-specific lethality of F1 progeny

274 [36]. The cellular basis of this lethality is poorly understood. With MAGIC, one may generate
275 mixed cell populations that are homozygous or heterozygous for species-specific alleles in the
276 same hybrid embryo or larva, in which the relative fitness of the three cell populations can be
277 compared. Similarly, MAGIC could complement genome-wide association studies (GWAS)
278 using wild-derived isogenic strains and provide much more mechanistic detail. Such strains as
279 those in the *Drosophila* Genetic Reference Panel (DGRP) [42] have been very useful for
280 discovering loci that are responsible for phenotypic variations. MAGIC can be combined with
281 these strains to analyze the effects of homozygosity of specific variants at the cell biology level
282 [8]. In addition, MAGIC can be combined with the *Drosophila* deficiency kit for rapid genome-
283 wide mosaic screens. A deficiency exhibiting a desired phenotype in such screens can be further
284 dissected with smaller deficiencies within the deleted region or existing mutations in candidate
285 genes. In this way, the convenience of MAGIC could significantly accelerate phenotype-based
286 gene discovery. Lastly, because the crossover site in MAGIC can be user-defined, one can easily
287 generate gRNA-markers that induce somatic recombination at specific genome locations. Such
288 flexibility could be useful for mapping undefined genetic loci that are responsible for certain
289 phenotypes, especially in non-traditional model organisms.

290 **MATERIALS AND METHODS:**

291 **Fly Stocks and Husbandry**

292 See the Key Resource Table (Table S1) for details of fly stocks used in this study. Most fly lines
293 were either generated in the Han lab or obtained from the Bloomington *Drosophila* Stock Center.
294 *lethal hybrid rescue* (*lhr*) mutant *D. Simulans* was a gift from Dr. Dan Barbash. All flies were
295 grown on standard yeast-glucose medium, in a 12:12 light/dark cycle, at 25°C unless otherwise
296 noted. Virgin males and females for mating experiments were aged for 3-5 days.

297 To generate and label pMAGIC clones in larval peripheral sensory neurons, we used
298 either *RabX4-Gal4 UAS-MApHS* (for gRNA-markers on chromosomes X, II, and IV) or *21-7-*
299 *Gal4 UAS-MApHS* (for gRNA-markers on chromosome III) combined with *zk-cas9*. To count
300 peripheral sensory neuronal clones on the larval body wall, third instar larvae were mounted
301 laterally on slides and then counted in segment A1-A7 under a Nikon SMZ18 stereomicroscope.
302 pMAGIC clones were induced and labeled by *RabX4-Gal4 UAS-MApHS* combined with *ey-cas9*
303 in the fly adult brain, by *tub-Gal4 UAS-mCD8-GFP* combined with *vas-cas9* in larval brains,

304 imaginal discs, fat bodies, guts, and trachea, by *repo-Gal4 UAS-mCD8-GFP* combined with
305 *gcm-cas9* in glia, by *pxn-Gal4 UAS-tdTom* combined with *Act-cas9* in hemocytes, by *tub-Gal4*
306 *UAS-mCD8-GFP* combined with *zk-cas9* in larval motor neurons, by *R38F11-Gal4 UAS-tdTom*
307 combined with *zk-cas9* in the larval epidermis. To induce nMAGIC clones in wing imaginal
308 discs of interspecific hybrid animals, we use *gRNA-42A4(BFP)*; *hh-cas9* virgin females of *D.*
309 *melanogaster* to cross with Lhr^{1} [43] *D. simulans* males.

310 **Molecular Cloning**

311 *MAGIC gRNA cloning vectors:* pMAGIC gRNA-marker vectors constructed in this study include
312 pAC-U63-gRNA2.1-ubiGal80(DE)-His2Av, pAC-U63-gRNA2.1-tubGal80(DE)-His2Av and
313 pAC-U63-gRNA2.1-tubGal80(DE)-SV40. To make pAC-U63-gRNA2.1-ubiGal80(DE)-His2Av,
314 a fragment containing gRNA2.1 scaffold (gRNA2.1) and U6 3' flanking sequence (U63fl) was
315 first used to replace gRNA2.1-QtRNA-Gal80(TS)-gRNA2.1-U63fl in pAC-U63-QtgRNA2.1-8R
316 (Addgene 170514) [17]. Then a destabilization sequence (DE) containing a GS linker, amino
317 acids (AAs) 422-461 of mouse ornithine decarboxylase [21], 2X RNA destabilizing nonamer
318 (TTATTTATTgatccTTATTTATT) [21] was added to the C-terminus of Gal80 in frame. To
319 make pAC-U63-gRNA2.1-tubGal80(DE)-His2Av, a 2.6 kb *tub* enhancer was amplified from
320 pENTR221-tubP [16] by PCR and used to replace the *ubi* enhancer in pAC-U63-gRNA2.1-
321 ubiGal80(DE)-His2Av. To make pAC-U63-gRNA2.1-tubGal80(DE)-SV40, a SV40 polyA
322 sequence was amplified from pAPIC-PHCS [22] and used to replace the His2Av polyA in pAC-
323 U63-gRNA2.1-ubiGal80(DE)-His2Av. To make the nMAGIC gRNA-marker vector pAC-U63-
324 gRNA2.1-tubBFP(HA), the gRNA2.1-U63fl fragment was first used to replace gRNA2.1-
325 QtRNA-BFP(TS)-gRNA2.1-U63fl in pAC-U63-QtgRNA2.1-BR (Addgene 170513) [17]. The
326 *tub* enhancer was then used to replace the *ubi* enhancer. Lastly, a synthetic DNA fragment
327 (GenScript) encoding 3X HA was used to replace the nuclear localization signal at the N-
328 terminus of mTagBFP. Cloning was carried out by ligation with T4 ligase or NEBuilder DNA
329 Assembly reactions (New England Biolabs Inc.).

330 *MAGIC gRNA expression vectors:* 33 gRNA expression vectors were constructed with the
331 corresponding gRNA cloning vectors as listed in Table 1 according to published protocols [17].
332 Briefly, for each expression vector, two primers containing appropriate gRNA target sequences
333 (Table S2) were used to amplify a fragment consisting of 3' end of U6:3 promotor, the first

334 target sequence (TS1), gRNA2.1, $tRNA^{Q}$, the second target sequence (TS2), and the beginning
335 sequence of gRNA2.1 with pAC-U63-QtgRNA2.1-BR as the PCR template. The PCR product
336 was then assembled with SapI-digested gRNA cloning vectors using NEBuilder DNA Assembly.

337 Injections were carried out by Rainbow Transgenic Flies (Camarillo, CA 93012 USA) or
338 Genetivision (Stafford, TX 77477) to transform flies through φC31 integrase-mediated
339 integration into attP docker sites. The 3xP3-RFP selection marker in gRNA-markers inserted at
340 the attP[ZH-102D] site were removed by crossing to Cre.

341 **Live Imaging**

342 Live imaging of larval epidermal cells, sensory neurons, and hemocytes was performed as
343 previously described [44]. Animals were collected at 96 (for late third larvae) or 120 hours AEL
344 (for wandering third instar larvae) hours after egg-laying (AEL) and mounted in glycerol on a
345 slide with vacuum grease as a spacer. Animals were imaged using a Leica SP8 confocal
346 microscope with a 40X NA1.3 oil objective, pinhole size 2 airy units, and a z-step size of 1 µm.
347 For epidermis, images were taken at the dorsal midline of A2 and A3 segments. For dendritic
348 arborization neurons, images were taken from A1 to A7 hemi-segments.

349 For imaging sensory neurons in pupae, newly formed pupae were collected and incubated
350 at 25 °C. After 16 hours, the pupal cases were carefully removed, and the pupae were mounted
351 dorsal side up on slides with halocarbon oil beneath a coverslip. Double-sided tape was used as a
352 spacer. The mounted pupae were imaged using a Leica SP8 confocal microscope with a 40X
353 NA1.3 oil objective.

354 **Imaging of wing discs and other larval tissues**

355 Larval dissections were performed as described previously [40]. Briefly, wandering third instar
356 larvae were dissected in a small petri dish filled with cold phosphate-buffered saline (PBS). The
357 anterior half of the larva was inverted. To prepare imaginal discs, trachea and gut were removed.
358 Samples were then transferred to 4% formaldehyde in PBS and fixed for 20 minutes at room
359 temperature. After washing with PBS, the tissues were stained in DAPI (1:1000) in 0.2% PBST
360 (PBS with 0.2% Triton X-100) for 5 minutes. The tissues were washed again in PBST and
361 mounted in SlowFade Diamond Antifade Mountant (Thermo Fisher Scientific) on a glass slide.

362 A coverslip was lightly pressed on top. Imaginal discs were imaged using a Leica SP8 confocal
363 microscope with a 20X NA0.8 oil objective.

364 **Adult brain imaging**

365 Flies were aged for 1 day after eclosion. Brains were dissected in PBS at room temperature and
366 then fixed in 4% paraformaldehyde in PBS with constant circular rotation for 20 minutes at room
367 temperature. The brains were subsequently washed in 0.2% PBST and mounted on a glass slide
368 under a glass coverslip. Vacuum grease was used as a spacer between the coverslip and the slide.
369 Brains were imaged using a Leica SP8 confocal microscope with a 40X NA1.3 oil objective.

370 **Larval fillet preparation**

371 Larval fillet dissection was performed on a petri dish half-filled with PMDS gel. Wandering third
372 instar larvae were pinned on the dish in PBS dorsal-side up and then dissected to expand the
373 body wall. PBS was then removed and 4% formaldehyde in PBS was added to fix larvae for 15
374 minutes at room temperature. For VGlut staining, the fillets were fixed in Bouin's solution for 5
375 minutes at room temperature. Fillets were rinsed and then washed at room temperature in PBS
376 for 20 minutes or until the yellow color from Bouin's solution faded. After immunostaining, the
377 head and tail of fillets were removed, and the remaining fillets were placed in SlowFade
378 Diamond Antifade Mountant on a glass slide. A coverslip was lightly pressed on top. Larval
379 fillets were imaged using a Leica SP8 confocal microscope with a 40X NA1.3 oil objective.

380 **Immunohistochemistry**

381 Larval brains and larval fillets were rinsed and washed at room temperature in 0.2% PBST after
382 fixation. The samples were then blocked in PBST with 5% normal donkey serum (NDS) for 1
383 hour before incubating with appropriate primary antibodies in the blocking solution. Brains were
384 stained for 2 hours at room temperature, and fillets were stained overnight at 4°C. After
385 additional rinsing and washing, the samples were incubated with secondary antibodies for 2
386 hours at room temperature. The samples were then rinsed and washed again before mounting and
387 imaging. Primary antibodies used in this study are mouse anti-Repo antibody 8D12 (1:50
388 dilution), mouse anti-Brp antibody nc82 (1:100 dilution), rabbit anti-VGlut (1:200 dilution) [39],
389 mouse anti-HA antibody (12CA5, 1:100), and goat anti-HRP conjugated with Cy3 (1:200).

Secondary antibodies include donkey anti-mouse antibody conjugated with Cy5 (1:400) and donkey anti-rabbit antibody conjugated with Cy5 (1:400).

Image Analysis and Quantification

ImageJ analyses were conducted in Fiji/ImageJ. To compare brightness of clones in sensory neurons and epidermal cells, clones were detected based on thresholds to generate masks. The clone brightness within the masks was then measured as mean pixel intensity. To quantify clones in wing discs, 2-3 slices of optical sections in the middle of the disc were projected into a 2-dimensional (2D) image. Clones were detected based on a fixed threshold to generate masks, and the total area of clones in the wing pouch of each disc was measured.

The tracing and measurement of da neuron dendrites were done as previously described in detail [44]. Briefly, dendrites were segmented using local thresholding. The segments were then converted into single-pixel-width skeletons. The total length of skeletons was calculated based on pixel distance. Normalized dendrite length was calculated as dendritic length (μm)/segment width (μm).

Statistical Analysis

One-way analysis of variance (ANOVA) with Tukey's honest significant difference (HSD) test was used when dependent variable was normally distributed and there was approximately equal variance across groups. Student's t-test was used when two groups are compared. For additional information on the number of samples, see figure legends. R studio was used for all statistical analyses.

ACKNOWLEDGMENTS

We thank Dion Dickman, Marcus Smolka, and Developmental Studies Hybridoma Bank (DSHB) for antibodies; Dan Barbash, Ethan Bier, and Bloomington *Drosophila* Stock Center for fly stocks; Dan Barbash and Tianzhu Xiong for advice on interspecific crosses; Claire Ho and Christina Breneman for helping to establish and test transgenes; Dan Barbash and Mariana Wolfner for feedback on the manuscript.

AUTHOR CONTRIBUTIONS

Conceptualization: Chun Han, Yifan Shen, Ann Yeung

Data curation: Yifan Shen, Ann Yeung, Elizabeth Korn, Rhiannon Clements, Parker Jarman

Formal analysis: Yifan Shen, Ann Yeung, Rhiannon Clements

Funding acquisition: Chun Han

Investigation: Yifan Shen, Ann Yeung, Elizabeth Korn, Rhiannon Clements, Xinchen Chen, Michael Sheen, Parker Jarman,

Methodology: Chun Han, Yifan Shen, Ann Yeung

Supervision: Chun Han, Yifan Shen, Ann Yeung, Rhiannon Clements, Elizabeth Korn

Resources: Yifan Shen, Payton Ditchfield, Bei Wang

Validation: Yifan Shen

Visualization: Yifan Shen, Ann Yeung, Rhiannon Clements

Writing – original draft: Chun Han, Yifan Shen

Writing – review & editing: Chun Han, Yifan Shen

REFERENCES

1. Germani F, Bergantinos C, Johnston LA. Mosaic Analysis in Drosophila. Genetics. 2018;208:4733-490. doi: 10.1534/genetics.117.300256.

2. Xu T, Rubin GM. The effort to make mosaic analysis a household tool. Development. 2012;139(24):4501-3. doi: 10.1242/dev.085183. PubMed PMID: 23172911; PubMed Central PMCID: PMCPMC3509720.

3. Griffin R, Binari R, Perrimon N. Genetic odyssey to generate marked clones in Drosophila mosaics. Proc Natl Acad Sci U S A. 2014;111(13):4756-63. Epub 20140312. doi: 10.1073/pnas.1403218111. PubMed PMID: 24623854; PubMed Central PMCID: PMCPMC3977257.

4. Golic KG, Lindquist S. The FLP recombinase of yeast catalyzes site-specific recombination in the Drosophila genome. Cell. 1989;59(3):499-509. doi: 10.1016/0092-8674(89)90033-0. PubMed PMID: 2509077.

5. Xu T, Rubin GM. Analysis of genetic mosaics in developing and adult Drosophila tissues. Development. 1993;117(4):1223-37. doi: 10.1242/dev.117.4.1223. PubMed PMID: 8404527.

6. Henner A, Ventura PB, Jiang Y, Zong H. MADM-ML, a mouse genetic mosaic system with increased clonal efficiency. PLoS One. 2013;8(10):e77672. Epub 20131015. doi: 10.1371/journal.pone.0077672. PubMed PMID: 24143253; PubMed Central PMCID: PMCPMC3797059.

7. Zong H, Espinosa JS, Su HH, Muzumdar MD, Luo L. Mosaic Analysis with Double Markers in Mice. Cell. 2005;121(3):479-92.

8. Allen SE, Koreman GT, Sarkar A, Wang B, Wolfner MF, Han C. Versatile CRISPR/Cas9-mediated mosaic analysis by gRNA-induced crossing-over for unmodified genomes. PLoS Biol. 2021;19(1):e3001061. Epub 20210114. doi: 10.1371/journal.pbio.3001061. PubMed PMID: 33444322; PubMed Central PMCID: PMCPMC7837743.

9. Thibault ST, Singer MA, Miyazaki WY, Milash B, Dompe NA, Singh CM, et al. A complementary transposon tool kit for Drosophila melanogaster using P and piggyBac. Nat Genet. 2004;36(3):283-7. Epub 2004/02/26. doi: 10.1038/ng1314. PubMed PMID: 14981521.

10. Hacker U, Nystedt S, Barmchi MP, Horn C, Wimmer EA. piggyBac-based insertional mutagenesis in the presence of stably integrated P elements in Drosophila. Proc Natl Acad Sci U S A. 2003;100(13):7720-5. Epub 2003/06/13. doi: 10.1073/pnas.1230526100. PubMed PMID: 12802016; PubMed Central PMCID: PMCPMC164654.

11. Bellen HJ, Levis RW, He Y, Carlson JW, Evans-Holm M, Bae E, et al. The Drosophila gene disruption project: progress using transposons with distinctive site specificities. Genetics. 2011;188(3):731-43. Epub 2011/04/26. doi: 10.1534/genetics.111.126995. PubMed PMID: 21515576; PubMed Central PMCID: PMCPMC3176542.

12. Staudt N, Molitor A, Somogyi K, Mata J, Curado S, Eulenberg K, et al. Gain-of-function screen for genes that affect Drosophila muscle pattern formation. PLoS Genet. 2005;1(4):e55. Epub 2005/10/29. doi: 10.1371/journal.pgen.0010055. PubMed PMID: 16254604; PubMed Central PMCID: PMCPMC1270011.

13. Bellen HJ, Levis RW, Liao G, He Y, Carlson JW, Tsang G, et al. The BDGP gene disruption project: single transposon insertions associated with 40% of Drosophila genes. Genetics. 2004;167(2):761-81. Epub 2004/07/09. doi: 10.1534/genetics.104.026427. PubMed PMID: 15238527; PubMed Central PMCID: PMCPMC1470905.

14. Yamamoto S, Jaiswal M, Charng WL, Gambin T, Karaca E, Mirzaa G, et al. A drosophila genetic resource of mutants to study mechanisms underlying human genetic diseases. Cell. 2014;159(1):200-14. Epub 2014/09/27. doi: 10.1016/j.cell.2014.09.002. PubMed PMID: 25259927; PubMed Central PMCID: PMCPMC4298142.

15. Cook RK, Christensen SJ, Deal JA, Coburn RA, Deal ME, Gresens JM, et al. The generation of chromosomal deletions to provide extensive coverage and subdivision of the Drosophila melanogaster genome. Genome Biol. 2012;13(3):R21. Epub 2012/03/27. doi: 10.1186/gb-2012-13-3-r21. PubMed PMID: 22445104; PubMed Central PMCID: PMCPMC3439972.

16. Chen X, Wang B, Sarkar A, Huang Z, Ruiz NV, Yeung AT, et al. Phagocytosis-driven neurodegeneration through opposing roles of an ABC transporter in neurons and phagocytes. Sci Adv. 2025;11(11):eadr5448. Epub 20250312. doi: 10.1126/sciadv.adr5448. PubMed PMID: 40073145; PubMed Central PMCID: PMCPMC11900885.

17. Koreman GT, Xu Y, Hu Q, Zhang Z, Allen SE, Wolfner MF, et al. Upgraded CRISPR/Cas9 tools for tissue-specific mutagenesis in Drosophila. Proc Natl Acad Sci U S A. 2021;118(14). Epub 2021/03/31. doi: 10.1073/pnas.2014255118. PubMed PMID: 33782117; PubMed Central PMCID: PMCPMC8040800.

491 18. Lee T, Luo L. Mosaic analysis with a repressible cell marker for studies of gene function
492 in neuronal morphogenesis. Neuron. 1999;22(3):451-61. doi: 10.1016/s0896-6273(00)80701-1.
493 PubMed PMID: 10197526.

494 19. Han C, Song Y, Xiao H, Wang D, Franc NC, Jan LY, et al. Epidermal cells are the
495 primary phagocytes in the fragmentation and clearance of degenerating dendrites in Drosophila.
496 Neuron. 2014;81(3):544-60. Epub 2014/01/15. doi: 10.1016/j.neuron.2013.11.021. PubMed
497 PMID: 24412417; PubMed Central PMCID: PMCPMC3995171.

498 20. Li X, Zhao X, Fang Y, Jiang X, Duong T, Fan C, et al. Generation of destabilized green
499 fluorescent protein as a transcription reporter. J Biol Chem. 1998;273(52):34970-5. doi:
500 10.1074/jbc.273.52.34970. PubMed PMID: 9857028.

501 21. Zubiaga AM, Belasco JG, Greenberg ME. The nonamer UUAUUUAUU is the key AU-
502 rich sequence motif that mediates mRNA degradation. Mol Cell Biol. 1995;15(4):2219-30. doi:
503 10.1128/MCB.15.4.2219. PubMed PMID: 7891716; PubMed Central PMCID:
504 PMCPMC230450.

505 22. Han C, Jan LY, Jan YN. Enhancer-driven membrane markers for analysis of
506 nonautonomous mechanisms reveal neuron-glia interactions in Drosophila. Proc Natl Acad Sci U
507 S A. 2011;108(23):9673-8. Epub 2011/05/25. doi: 10.1073/pnas.1106386108. PubMed PMID:
508 21606367; PubMed Central PMCID: PMCPMC3111288.

509 23. Ji H, Sapar ML, Sarkar A, Wang B, Han C. Phagocytosis and self-destruction break down
510 dendrites of Drosophila sensory neurons at distinct steps of Wallerian degeneration. Proc Natl
511 Acad Sci U S A. 2022;119(4). Epub 2022/01/22. doi: 10.1073/pnas.2111818119. PubMed PMID:
512 35058357; PubMed Central PMCID: PMCPMC8795528.

513 24. Lopez Del Amo V, Juste SS, Gantz VM. A nickase Cas9 gene-drive system promotes
514 super-Mendelian inheritance in Drosophila. Cell Rep. 2022;39(8):110843. doi:
515 10.1016/j.celrep.2022.110843. PubMed PMID: 35613590; PubMed Central PMCID:
516 PMCPMC9190248.

517 25. Charng WL, Yamamoto S, Bellen HJ. Shared mechanisms between Drosophila peripheral
518 nervous system development and human neurodegenerative diseases. Curr Opin Neurobiol.
519 2014;27:158-64. Epub 20140422. doi: 10.1016/j.conb.2014.03.001. PubMed PMID: 24762652;
520 PubMed Central PMCID: PMCPMC4122633.

521 26. Menon KP, Carrillo RA, Zinn K. Development and plasticity of the Drosophila larval
522 neuromuscular junction. Wiley Interdiscip Rev Dev Biol. 2013;2(5):647-70. Epub 20130205.
523 doi: 10.1002/wdev.108. PubMed PMID: 24014452; PubMed Central PMCID:
524 PMCPMC3767937.

525 27. Chou VT, Johnson SA, Van Vactor D. Synapse development and maturation at the
526 drosophila neuromuscular junction. Neural Dev. 2020;15(1):11. Epub 20200802. doi:
527 10.1186/s13064-020-00147-5. PubMed PMID: 32741370; PubMed Central PMCID:
528 PMCPMC7397595.

529 28. Daniels RW, Collins CA, Gelfand MV, Dant J, Brooks ES, Krantz DE, et al. Increased
530 expression of the Drosophila vesicular glutamate transporter leads to excess glutamate release
531 and a compensatory decrease in quantal content. J Neurosci. 2004;24(46):10466-74. doi:

532 10.1523/JNEUROSCI.3001-04.2004. PubMed PMID: 15548661; PubMed Central PMCID:
533 PMCPMC6730318.

534 29. Kittel RJ, Wichmann C, Rasse TM, Fouquet W, Schmidt M, Schmid A, et al. Bruchpilot
535 promotes active zone assembly, Ca2+ channel clustering, and vesicle release. Science.
536 2006;312(5776):1051-4. Epub 20060413. doi: 10.1126/science.1126308. PubMed PMID:
537 16614170.

538 30. Wagh DA, Rasse TM, Asan E, Hofbauer A, Schwenkert I, Durrbeck H, et al. Bruchpilot,
539 a protein with homology to ELKS/CAST, is required for structural integrity and function of
540 synaptic active zones in Drosophila. Neuron. 2006;49(6):833-44. doi:
541 10.1016/j.neuron.2006.02.008. PubMed PMID: 16543132.

542 31. Brown HL, Cherbas L, Cherbas P, Truman JW. Use of time-lapse imaging and dominant
543 negative receptors to dissect the steroid receptor control of neuronal remodeling in Drosophila.
544 Development. 2006;133(2):275-85. Epub 20051214. doi: 10.1242/dev.02191. PubMed PMID:
545 16354717.

546 32. Williams DW, Truman JW. Cellular mechanisms of dendrite pruning in Drosophila:
547 insights from in vivo time-lapse of remodeling dendritic arborizing sensory neurons.
548 Development. 2005;132(16):3631-42. Epub 20050720. doi: 10.1242/dev.01928. PubMed PMID:
549 16033801.

550 33. Goldsmith SL, Shimell M, Tauscher P, Daly SM, Shimmi O, O'Connor MB, et al. New
551 resources for the Drosophila 4th chromosome: FRT101F enabled mitotic clones and Bloom
552 syndrome helicase enabled meiotic recombination. G3 (Bethesda). 2022;12(4). doi:
553 10.1093/g3journal/jkac019. PubMed PMID: 35084488; PubMed Central PMCID:
554 PMCPMC8982423.

555 34. Riddle NC, Minoda A, Kharchenko PV, Alekseyenko AA, Schwartz YB, Tolstorukov
556 MY, et al. Plasticity in patterns of histone modifications and chromosomal proteins in Drosophila
557 heterochromatin. Genome Res. 2011;21(2):147-63. Epub 20101222. doi: 10.1101/gr.110098.110.
558 PubMed PMID: 21177972; PubMed Central PMCID: PMCPMC3032919.

559 35. Chakraborty M, Chang CH, Khost DE, Vedanayagam J, Adrion JR, Liao Y, et al.
560 Evolution of genome structure in the Drosophila simulans species complex. Genome Res.
561 2021;31(3):380-96. Epub 20210209. doi: 10.1101/gr.263442.120. PubMed PMID: 33563718;
562 PubMed Central PMCID: PMCPMC7919458.

563 36. Barbash DA. Ninety years of Drosophila melanogaster hybrids. Genetics. 2010;186(1):1-
564 8. doi: 10.1534/genetics.110.121459. PubMed PMID: 20855573; PubMed Central PMCID:
565 PMCPMC2940278.

566 37. Port F, Chen HM, Lee T, Bullock SL. Optimized CRISPR/Cas tools for efficient germline
567 and somatic genome engineering in Drosophila. PNAS. 2014;111(29):E2967-E76. doi:
568 10.1073/pnas.1405500111.

569 38. Garcia-Marques J, Espinosa-Medina I, Ku K-Y, Yang C-P, Koyama M, Yu H-H, et al. A
570 programmable sequence of reporters for lineage analysis. Nature Neuroscience. 2020. doi:
571 10.1038/s41593-020-0676-9.

572 39. Chen X, Perry S, Fan Z, Wang B, Loxterkamp E, Wang S, et al. Tissue-specific knockout
573 in the Drosophila neuromuscular system reveals ESCRT's role in formation of synapse-derived

extracellular vesicles. PLoS Genet. 2024;20(10):e1011438. Epub 20241010. doi: 10.1371/journal.pgen.1011438. PubMed PMID: 39388480.

40. Poe AR, Wang B, Sapar ML, Ji H, Li K, Onabajo T, et al. Robust CRISPR/Cas9-Mediated Tissue-Specific Mutagenesis Reveals Gene Redundancy and Perdurance in Drosophila. Genetics. 2019;211(2):459-72. Epub 2018/12/07. doi: 10.1534/genetics.118.301736. PubMed PMID: 30504366; PubMed Central PMCID: PMCPMC6366929.

41. Chen HM, Yao X, Ren Q, Chang CC, Liu LY, Miyares RL, et al. Enhanced Golic+: highly effective CRISPR gene targeting and transgene HACKing in Drosophila. Development. 2020;147(11). Epub 20200611. doi: 10.1242/dev.181974. PubMed PMID: 32467238.

42. MacKay TFC, Richards S, Stone EA, Barbadilla A, Ayroles JF, Zhu D, et al. The Drosophila melanogaster Genetic Reference Panel. Nature. 2012;482(7384):173-8. doi: 10.1038/nature10811.

43. Brideau NJ, Flores HA, Wang J, Maheshwari S, Wang X, Barbash DA. Two Dobzhansky-Muller genes interact to cause hybrid lethality in Drosophila. Science. 2006;314(5803):1292-5. doi: 10.1126/science.1133953. PubMed PMID: 17124320.

44. Poe AR, Tang L, Wang B, Li Y, Sapar ML, Han C. Dendritic space-filling requires a neuronal type-specific extracellular permissive signal in Drosophila. PNAS. 2017:E8062-E71. doi: 10.1073/pnas.1707467114.

594 **FIGURES**

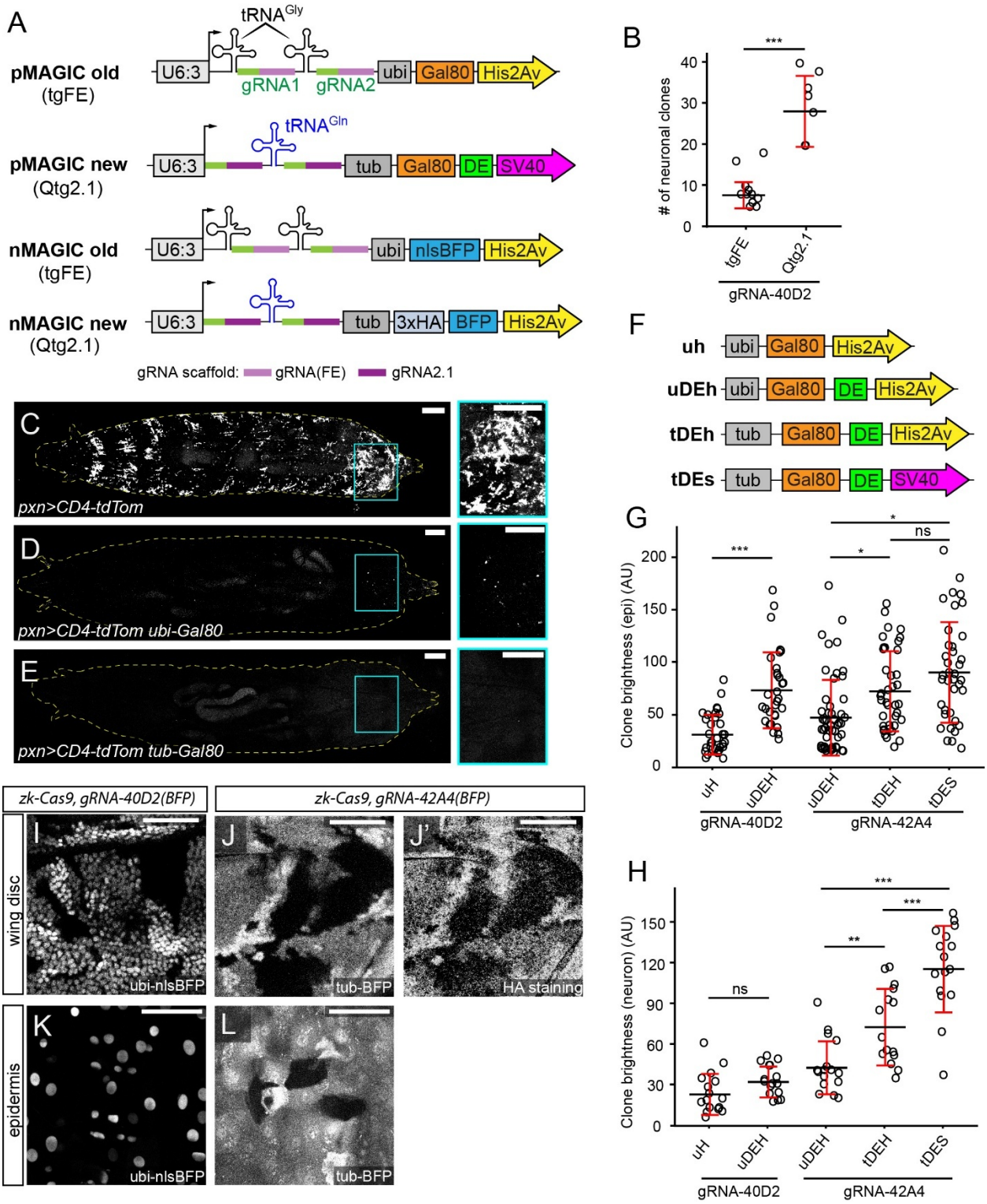

595

596 **Figure 1. New gRNA-marker designs improve pMAGIC and nMAGIC.**

597 (A) Original and new designs of gRNA-markers for pMAGIC and nMAGIC. (B) Comparison of
598 clone frequency in larval sensory neurons between two gRNA designs. The number represents

clones between A1 and A7 segments on one side of each larva. n = larvae number: tgFE (n=10), Qtg2.1 (n=10). (C-E) Labeling of hemocytes in whole 3rd instar larvae by *pxn*^{Gal4}>*CD4-tdTom* alone (C) or together with *ubi-Gal80* (D) or *tub-Gal80* (E). The panels on the right show enlarged views of the boxed regions. (F) Designs of Gal80 variants tested in pMAGIC gRNA-markers. (G) The brightness of epidermal clones labeled by pMAGIC gRNA-markers. n = image numbers: gRNA-40D2-uH (n = 32), gRNA-40D2-uDEH (n = 31), gRNA-42A4-uDEH (n = 52), gRNA-42A4-tDEH (n = 39), gRNA-42A4-tDES (n = 38). (H) The brightness of neuronal clones labeled by pMAGIC gRNA-markers. n = neuron numbers: gRNA-40D2-uH (n = 16), gRNA-40D2-uDEH (n = 16), gRNA-42A4-uDEH (n = 16), gRNA-42A4-tDEH (n = 15), gRNA-42A4-tDES (n = 16). (I) Portion of a larval wing disc containing nMAGIC clones visualized by nlsBFP. (J and J') Portion of a wing disc containing nMAGIC clones labeled by cytosolic BFP (J) and HA staining (J'). (K) Epidermal clones on the larva body wall labeled by nlsBFP. (L) Epidermal clones visualized by cytosolic BFP. In all plots, black bar, mean; red bar, SD; AU, arbitrary unit. Student's t-test in (B); one-way analysis of variance (ANOVA) and Tukey's honest significant difference (HSD) test in (G) and (H). *p≤0.05, **p≤0.01, ***p≤0.001, ns, not significance. For (C-E), scale bar, 300 µm. For (I-M), scale bar, 100 µm.

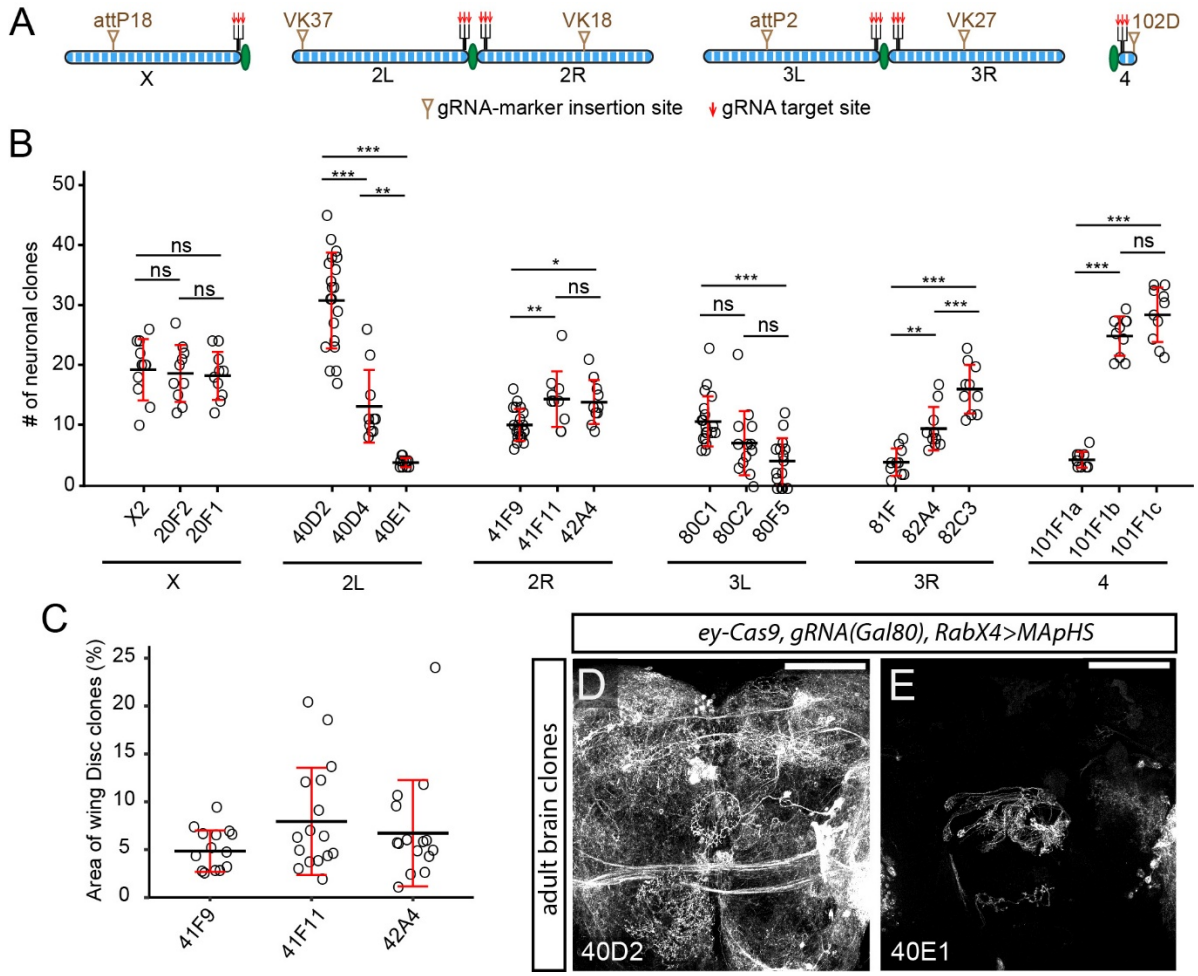

Figure 2. A genome-wide gRNA-marker kit suits diverse needs of clone frequency.

617 (A) Scheme of gRNA-marker insertion sites and target sites on *Drosophila* chromosomes. (B)
618 Comparison of clone frequencies of all pMAGIC gRNA-markers in larval sensory neurons,
619 clones are labeled using *RabX4-Gal4 UAS-MApHs* (for Chromosome X, II and IV) or *21-7-Gal4*
620 *UAS-MApHs* (for Chromosome III). n = larvae number: X2 (n = 10), 20F2 (n = 10), 20F1(n =
621 10), 40D2 (n = 20), 40D4 (n = 10), 40E1 (n = 10), 41F9 (n = 20), 41F11 (n = 10), 42A4 (n =
622 10), 80C1 (n = 20), 80C2 (n = 14), 80F5 (n = 15), 81F (n = 10), 82A4 (n = 10), 82C3 (n = 10),
623 101F1a (n = 10), 101F1b (n = 10), 101F1c (n = 10). (C) Comparison of clone areas in larval
624 wing discs labeled by nMAGIC gRNA-markers on 2R. n = wing disc number: 41F9 (n = 14),
625 41F11 (n = 16), 42A4 (n = 15). (D and E) Neuronal clones in the central part of the adult brain
626 induced by pMAGIC gRNA-markers *gRNA-40D2* (D) and *gRNA-40E1* (E). In all plots, black
627 bar, mean; red bar, SD. One-way ANOVA and Tukey's HSD test. *p≤0.05, **p≤0.01,
628 ***p≤0.001, ns, not significance. For (D) and (E), scale bar 100 µm.

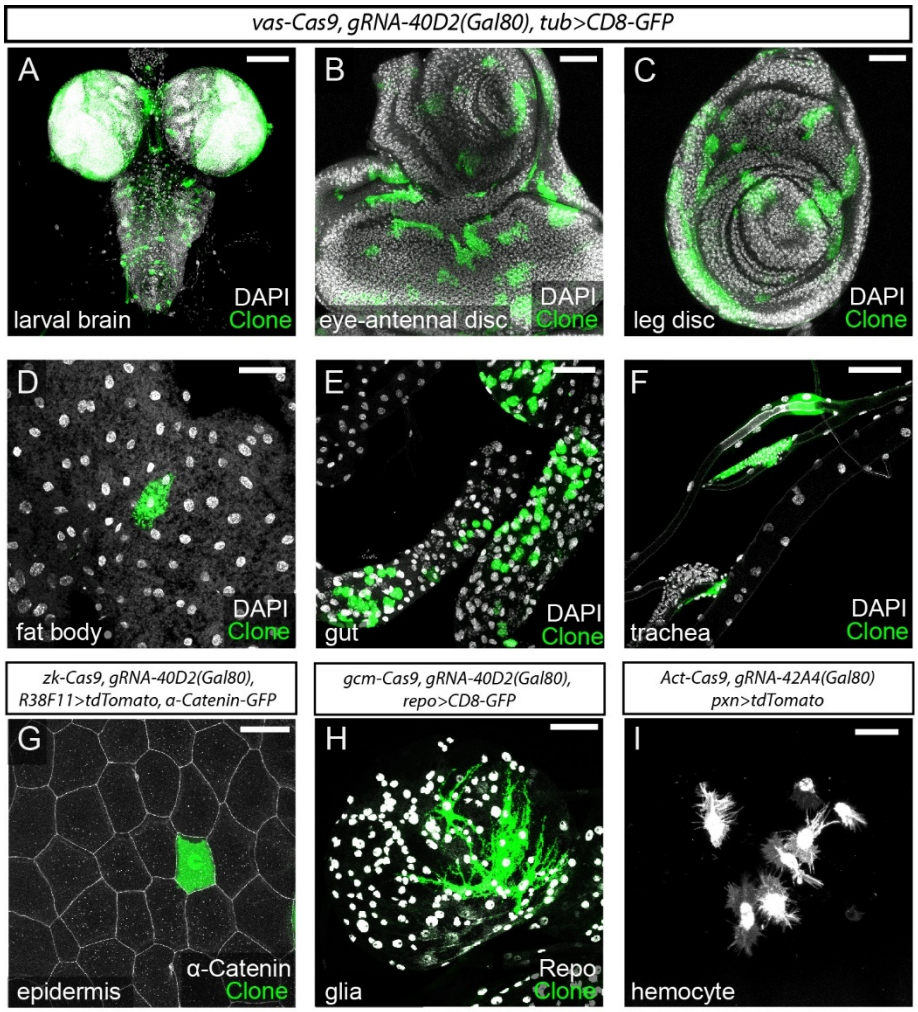

629

630 **Figure 3. MAGIC allows clonal analysis in diverse tissues and cell types.**
631 (A-F) pMAGIC clones induced in different tissues by *vas-Cas9 gRNA-40D2(Gal80)* and labeled
632 by *tub-Gal4 UAS-CD8-GFP* (green). DAPI staining (white) shows all nuclei. (G) A pMAGIC
633 epidermal clone on the larval body wall induced by *zk-Cas9 gRNA-40D2(Gal80)* and labeled by

634 *R38F11-Gal4 UAS-tdTom* (green). Epidermal junctions are labeled by *α-Catenin-GFP* (white).
635 (H) pMAGIC glia clones in the larval brain induced by *gcm-Cas9 gRNA-40D2(Gal80)* and
636 labeled by *repo-Gal4 UAS-CD8-GFP* (green). Glial nuclei are labeled by Repo staining (white).
637 (I) pMAGIC hemocyte clones induced by *Act-Cas9 gRNA-40D2(Gal80)* and labeled by *pxn-*
638 *Gal4 UAS-tdTom*. For figure A, D-F, H, scale bar 100 µm. For figure B-C, G, scale bar 50 µm.
639 For Figure I, scale bar 25 µm.

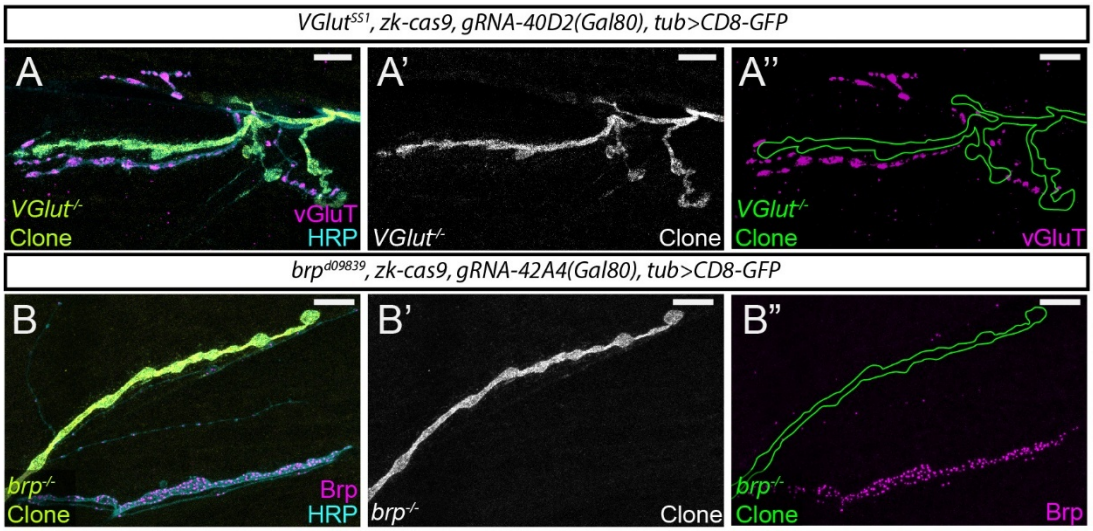

640
641 **Figure 4. MAGIC facilitates clonal analysis at the NMJ.**
642 (A-A") pMAGIC clones of *VGlut*^{1} mutation in motor neurons at the neuromuscular junction.
643 Clones were induced by *zk-Cas9 gRNA-40D2(Gal80)* and labeled by *tub-Gal4 UAS-CD8-GFP*. ,
644 The loss of VGlut is confirmed by VGlut staining. The mutant clones are outlined in (A"). (B-
645 B") A pMAGIC clone of *brp*^{d09839} mutation in a motor neuron at the neuromuscular junction.
646 Clones were induced by *zk-Cas9 gRNA-42A4(Gal80)* and labeled by *tub-Gal4 UAS-CD8-GFP*.
647 The loss of Brp is confirmed by Brp staining. The mutant clone is outlined in (B"). In both
648 experiments, HRP staining shows all axons. Scale bars, 10 µm.

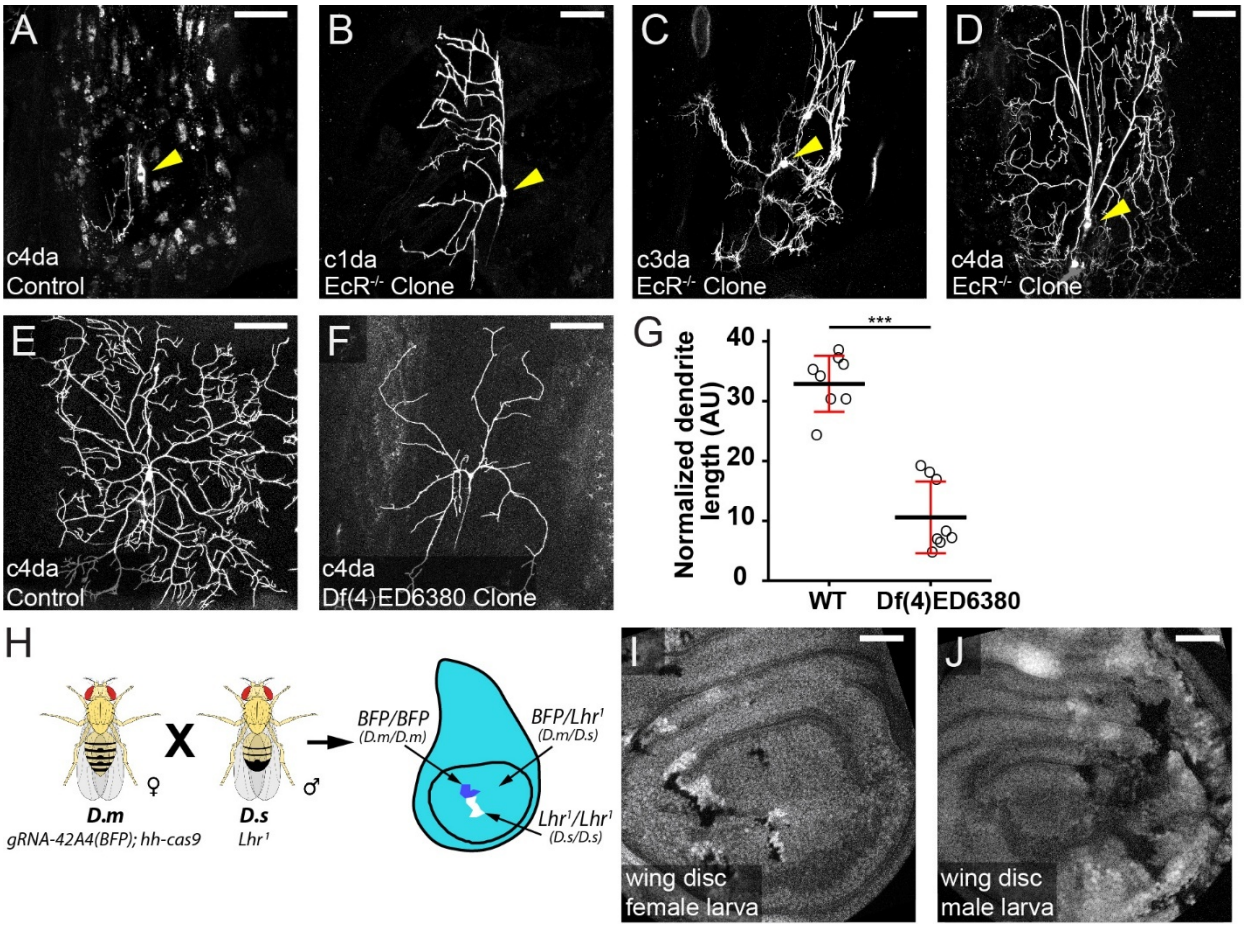

Figure 5. MAGIC enables clonal analysis of pericentromeric genes, 4th chromosome-associated mutations, and in interspecific hybrid animals.

(A) A WT pMAGIC class IV da neuron clone exhibiting complete dendrite pruning at 16 hours APF. (B-D) pMAGIC clones of *EcR*^{M554fs} mutation in da neurons imaged at 16 hours APF, exhibiting the lack of pruning (B and D) or apoptosis (C). In (A-D), the clones were induced by *zk-cas9* with *gRNA-41F9(Gal80)* and labeled by *RabX4-Gal4 UAS-MApHS*. Neuronal cell bodies are indicated by arrows. MApHS contains pHluorin and tdTom [19], but only tdTom signals are shown. The signals in epidermal cells (A) were due to engulfment of pruned dendrites by epidermal cells [19]. (E and F) WT (E) and *Df(4)ED6380* (F) pMAGIC clones in C4da neurons induced by *zk-cas9 gRNA-101Fc(Gal80)* and labeled by *RabX4-Gal4 UAS-MApHS*. Only tdTom signals are shown. (G) Normalized dendrite length of WT clones and deficiency clones. Black bar, mean; red bar, SD. Student's t-test. ***$p \leq 0.001$. (H) Scheme for interspecific crosses between *D. melanogaster* (*D.m*) and *D. simulans* (*D.s*). (I and J) Wing discs from male (I) and female (J) progeny carrying clones. Scale bars, 50 µm.

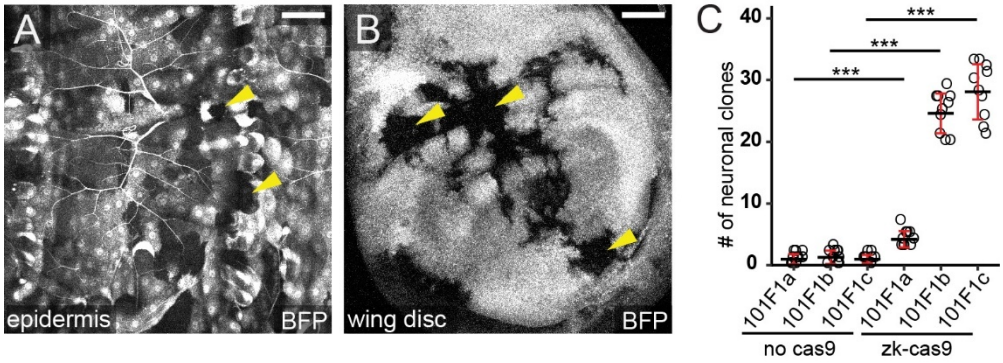

Figure S1. Transgenic markers on the 4th chromosome show uneven expression. (A-B) Representative epidermal (A) and wing disc (B) images showing uneven expression of *gRNA-101F1c(BFP)* inserted at *attP*^{102D} on the 4th chromosome. Yellow arrowheads point to cells lacking BFP expression. Scale bars, 50 µm. (C) Frequency of labeled neurons by indicated gRNA(Gal80) in the absence and presence of Cas9. The *zk-Cas9* dataset is the same as that for chromosome 4 in Figure 2B. Black bar, mean; red bar, SD. One-way ANOVA and HSD test. ***$p \leq 0.001$.

Table 1. gRNA-marker collection

Chr Arm	target site	gRNA location	pMAGIC vector	nMAGIC vector	clone frequency
2L	40D2	attP[VK00037]	*pAC-U63-gRNA2.1-ubiGal80(DE)-His2Av*	*pAC-U63-tgRNA-nlsBFP**	31
2L	40D4	attP[VK00037]	*pAC-U63-tgRNA-Gal80**	*pAC-U63-tgRNA-nlsBFP**	13
2L	40E1	attP[VK00037]	*pAC-U63-tgRNA-Gal80**	*pAC-U63-tgRNA-nlsBFP**	4
2R	41F9	attP[VK00018]	*pAC-U63-gRNA2.1-ubiGal80(DE)-His2Av*	*pAC-U63-gRNA2.1-tubBFP(HA)*	10
2R	41F11	attP[VK00018]	*pAC-U63-gRNA2.1-ubiGal80(DE)-His2Av*	*pAC-U63-gRNA2.1-tubBFP(HA)*	14
2R	42A4	attP[VK00018]	*pAC-U63-gRNA2.1-tubGal80(DE)-SV40*	*pAC-U63-gRNA2.1-tubBFP(HA)*	14
3L	80F5	attP2	*pAC-U63-gRNA2.1-tubGal80(DE)-His2Av*	*pAC-U63-gRNA2.1-tubBFP(HA)*	11
3L	80C2	attP2	*pAC-U63-gRNA2.1-tubGal80(DE)-His2Av*	*pAC-U63-gRNA2.1-tubBFP(HA)*	7
3L	80C1	attP2	*pAC-U63-gRNA2.1-tubGal80(DE)-His2Av*	*pAC-U63-gRNA2.1-tubBFP(HA)*	4
3R	81F	attP[VK00027]	*pAC-U63-gRNA2.1-tubGal80(DE)-His2Av*	*pAC-U63-gRNA2.1-tubBFP(HA)*	4
3R	82A4	attP[VK00027]	*pAC-U63-gRNA2.1-tubGal80(DE)-His2Av*	*pAC-U63-gRNA2.1-tubBFP(HA)*	10

3R	82C3	attP[VK00027]	*pAC-U63-gRNA2.1-tubGal80(DE)-His2Av*	*pAC-U63-gRNA2.1-tubBFP(HA)*	16
X	X2	attP18	*pAC-U63-gRNA2.1-tubGal80(DE)-SV40*	*pAC-U63-gRNA2.1-tubBFP(HA)*	19
X	20F1	attP18	*pAC-U63-gRNA2.1-tubGal80(DE)-SV40*	*pAC-U63-gRNA2.1-tubBFP(HA)*	18
X	20F2	attP18	*pAC-U63-gRNA2.1-tubGal80(DE)-SV40*	*pAC-U63-gRNA2.1-tubBFP(HA)*	19
IV	101F1-a	attP[ZH-102D]**	*pAC-U63-gRNA2.1-tubGal80(DE)-SV40*	*pAC-U63-gRNA2.1-tubBFP(HA)*	4
IV	101F1-b	attP[ZH-102D]**	*pAC-U63-gRNA2.1-tubGal80(DE)-SV40*	*pAC-U63-gRNA2.1-tubBFP(HA)*	25
IV	101F1-c	attP[ZH-102D]**	*pAC-U63-gRNA2.1-tubGal80(DE)-SV40*	*pAC-U63-gRNA2.1-tubBFP(HA)*	28

Clone frequencies are measured by averaging clone numbers in 10 laterally mounted 3rd instar larvae with pMAGIC gRNA-markers. Only clones in A1 to A7 segments of one side of each larva were counted.
*Previously published gRNA-markers.
**3xP3-RFP has been removed from these lines.

673